

would be expected in a chaotic system but instead converge to nearly identical values. There are several models (8, 9) that have successfully simulated the observed seasonal mean tropical rainfall with prescribed SST. This apparent lack of sensitive dependence on the initial conditions provides a scientific basis for long-range forecasting of tropical climate variations. As shown by several modeling and theoretical studies (10–13), reliable probabilistic estimates of extratropical predictability are also realizable but only in the case of large tropical SST anomalies.

There is not yet a rigorous explanation for why the tropical atmosphere has such a unique property. However, it is reasonable to conjecture that the latitudinal dependence of the rotational force and solar heating produce the unique structure of the large-scale tropical motion field that, for a given boundary condition of SST, is stable with respect to the internal changes.

In spite of the apparent high predictability of the tropical atmosphere, accurate or useful forecasts for tropical circulation and rainfall can be made only if the tropical SST itself is accurately predicted. The tropical Pacific Ocean also has the unique property that changes in the tropical ocean circulation and SST are not sensitively dependent on the initial conditions of the ocean and are determined by the overlying atmospheric conditions (14). Lack of sensitive dependence on initial conditions for the tropical atmosphere and tropical oceans separately does not necessarily imply that the coupled tropical ocean–atmosphere system is also predictable. However, climate research in the past two decades has shown that the coupled tropical ocean–atmosphere system is indeed predictable for several seasons (9, 15, 16). This suggests that, at least for certain regions of the tropics, the potential exists for making dynamic forecasts of climate anomalies several seasons in advance.

Several news stories have reported that the 1997–1998 El Niño and its global effects were successfully predicted several months in advance. This paper suggests that the successful prediction of 1997–1998 climate anomalies did not occur by chance, and large-scale global climate anomalies associated with all future large El Niño events should be predictable several months in advance. This will be possible because, even if the initiation of an El Niño event could not be predicted several months in advance—and there is no evidence yet that it could be—once an El Niño event has begun, its growth and maturation for the following 6 to 9 months appear to be predictable. The reason successful long-range predictions of global climate anomalies could not be made in the past was because there were neither accurate models of the

ocean and atmosphere to predict the SST and to calculate the associated changes in global circulation and rainfall nor sufficient observations for the tropical Pacific Ocean. The 1997–1998 El Niño event happened to occur just as the subsurface ocean observing system in the tropical Pacific was in place, and better models of the climate system had been developed. It is now clear that certain aspects of the climate system have far more predictability than was previously recognized. It also should be recognized that some aspects of the climate system will always be difficult to predict. For example, there has been no success in predicting subseasonal variations and, to the extent that they will influence the life cycle of El Niño events, our ability to predict the correct amplitude of El Niño events will also be limited. However, with further improved models and more accurate and extensive global observations, especially in and over the oceans, it should be possible to provide useful forecasts for seasonal mean climate.

References and Notes

1. E. N. Lorenz, *J. Atmos. Sci.* **20**, 130 (1963).
2. ———, *Chaos* (Univ. of Washington Press, Seattle, 1993), pp. 181–184.
3. B. P. Kirtman and D. G. DeWitt, *Mon. Weather Rev.* **125**, 1231 (1997).
4. P. Xie and P. Arkin, *J. Climate* **9**, 840 (1996).
5. J. Shukla *et al.*, *COLA Tech. Rep.* **50**, 1 (1997).
6. J. G. Charney and J. Shukla, *Monsoon Dynamics* (Cambridge Univ. Press, New York, 1981), pp. 99–109.
7. J. Shukla, *ECMWF Workshop Rep.* **21** (1981).
8. R. A. Kerr, *Science* **266**, 544 (1994).
9. L. Bengtsson *et al.*, *ibid.* **261**, 1026 (1993).
10. C. Brankovic, T. N. Palmer, L. Ferranti, *J. Climate* **7**, 217 (1994).
11. T. P. Barnett, *ibid.* **8**, 1005 (1995).
12. A. Kumar and M. P. Hoerling, *ibid.* **10**, 83 (1997).
13. K. Trenberth *et al.*, *J. Geophys. Res.* **103**, 14291 (1998).
14. R. Seager, *J. Phys. Ocean* **19**, 419 (1989).
15. National Research Council, *Accomplishments and Legacies of the TOGA Program* (National Academy Press, Washington, DC, 1996), pp. 66–75.
16. M. Latif *et al.*, *J. Geophys. Res.* **103**, 14375 (1998).
17. Thanks are due to L. Marx, D. Paolino, and J. L. Kinter for help in the calculation and analysis of model results and to L. Dolhancryk for help in preparation of the manuscript. Supported by the National Oceanic and Atmospheric Administration (NA76GPO258) and the National Science Foundation (ATM 9321354).

25 June 1998; accepted 15 September 1998

Climate and Groundwater Recharge During the Last Glaciation in an Ice-Covered Region

Urs Beyerle,* Roland Purtschert, Werner Aeschbach-Hertig, Dieter M. Imboden, Heinz H. Loosli, Rainer Wieler, Rolf Kipfer

A multitracer study of a small aquifer in northern Switzerland indicates that the atmosphere in central Europe cooled by at least 5°C during the last glacial period. The relation between oxygen isotope ratios ($\delta^{18}\text{O}$) and recharge temperatures reconstructed for this period is similar to the present-day one if a shift in the $\delta^{18}\text{O}$ value of the oceans during the ice age is taken into account. This similarity suggests that the present-day $\delta^{18}\text{O}$ -temperature relation can be used to reconstruct paleoclimate conditions in northern Switzerland. A gap in calculated groundwater age between about 17,000 and 25,000 years before the present indicates that during the last glacial maximum, local groundwater recharge was prevented by overlying glaciers.

Continental climate records from mid-latitude regions that experienced ice cover during the last glacial period are scarce. Ground-

waters have been used as paleoclimate archives in permanently ice-free regions (1–4). Here we present groundwater data from the Glatt Valley, Switzerland, which was ice-covered after a glacial advance during the last glacial maximum (5). The impact of glaciation on groundwater recharge and dynamics is not well known, but numerical models have shown that glaciers can dramatically change groundwater flow (6). In groundwater, past values of climate variables can be derived from the stable isotope composition of water molecules (7) and the concentrations of dissolved atmospheric noble gases (8).

U. Beyerle, W. Aeschbach-Hertig, D. M. Imboden, R. Kipfer, Department of Environmental Physics, Swiss Federal Institute of Technology (ETH) Zurich and Swiss Federal Institute of Environmental Science and Technology (EAWAG), 8600 Dübendorf, Switzerland. R. Purtschert and H. H. Loosli, Physics Institute, University of Berne, 3012 Berne, Switzerland. R. Wieler, Isotope Geology, Department of Earth Sciences, ETH Zurich, NO C61, 8092 Zurich, Switzerland.

*To whom correspondence should be addressed. E-mail: beyerle@eawag.ch

REPORTS

Besides the local air temperature, many factors control the isotopic composition of groundwater (9). In contrast, the concentrations of atmospheric noble gases dissolved in groundwater are determined mainly by the solubility equilibrium during infiltration, given by the mean local atmospheric pressure (specified by the altitude of the recharge area) and by the water temperature prevailing during recharge. The so-called noble gas temperature (NGT) is therefore a measure of the temperature at which groundwater equilibrated with the atmosphere during infiltration,

and it commonly corresponds to the mean annual air temperature (10). Consequently, information on stable isotopes and noble gases taken together allows one to evaluate the oxygen isotope ($\delta^{18}\text{O}$)-temperature relation over long time scales.

The deep Glatt Valley aquifer (GVA), situated about 100 m below ground level, is 15 km long, 3 km wide, and has an average thickness of 10 m (Fig. 1). It is formed of gravel and sand and has a permeability of 10^{-5} to 10^{-6} m s^{-1} (11). Poorly permeable Pleistocene sediments separate the GVA

from a shallow unconfined groundwater system, the Aathal aquifer. The presumed recharge area of the GVA is located near borehole 0 at an elevation of about 540 m. In 1995 and 1996, samples from boreholes tapping the GVA were collected by means of a submersed pump. Hydrochemistry, noble gases, radionuclides (^3H , ^{85}Kr , ^{37}Ar , ^{39}Ar , and ^{14}C) and stable isotope ratios ($\delta^{13}\text{C}$, $\delta^2\text{H}$, and $\delta^{18}\text{O}$) were measured (Table 1).

NGTs are calculated from noble gas concentrations by accounting for their temperature-dependent solubilities and for the com-

Fig. 1. (Top left) Map showing the location of the Glatt Valley, Switzerland. **(Center)** Detailed map of the study area showing boreholes 0 through 7. Open circles represent boreholes yielding a mixture of an older and a younger groundwater; solid circles represent boreholes without mixture; dash-dotted lines indicate location of profiles 1 and 2 (shown top right and bottom); and thin solid lines indicate the contours of the underlying molasse bedrock (shown at 50-m intervals). The presumed recharge area lies south-east of borehole 0, where the confining sediments outcrop (17). Arrows indicate the general direction of groundwater flow.

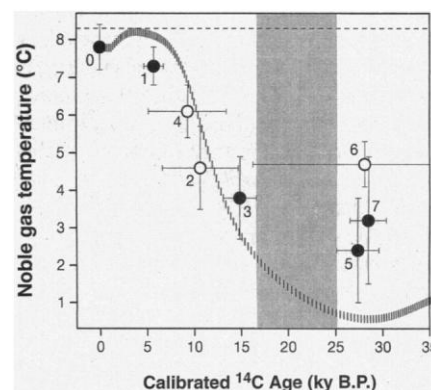
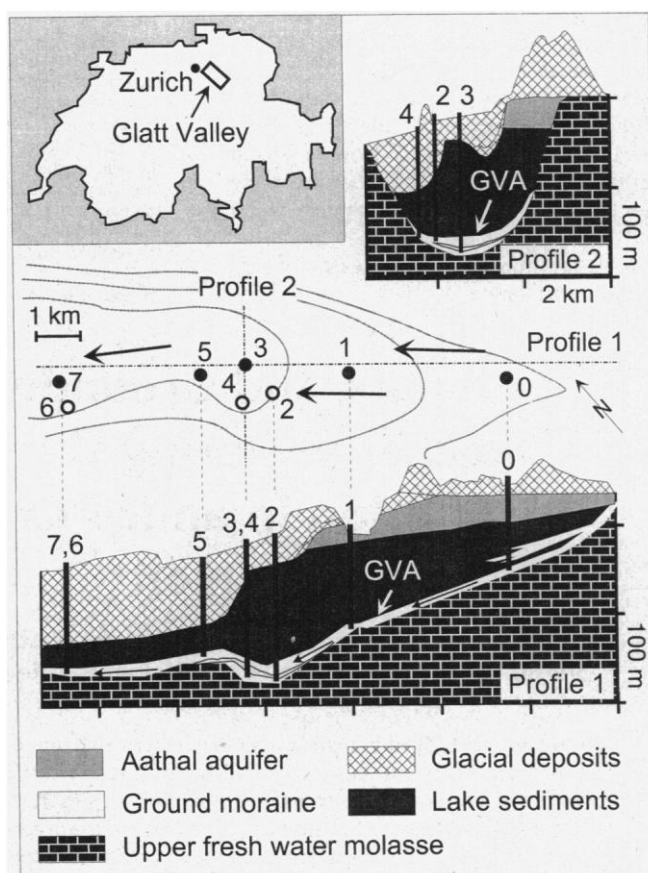


Fig. 2. NGT versus calibrated ^{14}C age. Error bars correspond to 1σ . The sample numbers refer to the boreholes shown in Fig. 1. Solid circles indicate samples without mixture. For samples containing a mixture of an older and a younger component (open circles), the values shown refer to the older component only. The horizontal dashed line indicates the modern mean annual air temperature of 8.3°C (17). No water was found for the period between 25 and 17 ky B.P. (shaded area). The curve is derived from a model that shows how a temperature evolution similar to that recorded in the oxygen isotope profiles of Greenland ice cores would be transferred through a dispersive flow system. The larger distance between the bars of the curve in the age range of the assumed recharge gap (from 25 to 17 ky B.P.) reflects the reduced probability of finding a water sample with a mean residence time between 25 and 17 ky B.P.

Table 1. Noble gas, stable and radioactive isotope, and chloride data from the GVA groundwater samples. Sampling locations are given in Fig. 1. ΔNe is the contribution of excess air to the Ne concentration normalized to the solubility equilibrium component at the temperature equal to the NGT. NGT is the noble gas temperature derived from Ne, Ar, Kr, and Xe by optimizing

temperature and excess air to minimize the sum of the weighted least-square difference between measured and predicted concentrations (27). ^{14}C , ^{39}Ar , and ^{85}Kr activities were measured by low-level counting (28). STP, standard temperature and pressure; pmc, percent modern carbon; TU, tritium unit; dpm, decay per minute; NA, not analyzed.

Borehole	$\delta^2\text{H}$ (‰)	$\delta^{18}\text{O}$ (‰)	$(\text{cm}^3 \text{ STP/g})$					ΔNe (%)	NGT (°C)	^{14}C (pmc)	^{13}C (‰)	^{39}Ar (% modern)	^3H (TU)	^{85}Kr (dpm/cm ³ STP Kr)	Cl^- ($\mu\text{mol/l}$)
			He (10^{-8})	Ne (10^{-7})	Ar (10^{-4})	Kr (10^{-8})	Xe (10^{-8})								
0	-70.0	-9.8	5.67	2.39	4.13	9.40	1.34	24	7.8 ± 0.6	78.9 ± 0.9	-15.1	114 ± 8	30.0 ± 1.3	29.8 ± 0.6	129.8
1	-70.6	-9.7	11.3	2.16	3.94	9.22	1.39	11	7.3 ± 0.5	22.1 ± 0.4	-10.3	9 ± 5	0.4 ± 0.1	0.8 ± 0.6	11.3
2	-71.2	-10.0	49.6	2.41	4.23	9.79	1.50	22	5.6 ± 0.7	24.5 ± 0.5	-11.1	27 ± 5	0.3 ± 0.1	NA	19.7
3	-80.5	-11.0	26.5	2.42	4.38	10.24	1.65	20	3.8 ± 1.1	9.2 ± 0.5	-11.0	12 ± 3	0.1 ± 0.1	0.4 ± 0.4	11.3
4	-73.1	-9.8	27.3	2.42	4.21	9.64	1.37	24	6.8 ± 0.6	39.3 ± 0.1	-14.7	54 ± 8	0.3 ± 0.1	0.6 ± 0.4	22.6
5	-85.5	-11.5	51.3	2.16	4.32	10.45	1.74	6	2.4 ± 1.4	1.7 ± 0.2	-8.1	NA	0.7 ± 0.1	NA	14.1
6	-74.4	-10.5	89.5	2.37	4.29	10.02	1.54	19	4.9 ± 0.6	5.1 ± 0.2	-10.3	35 ± 6	0.1 ± 0.1	NA	19.7
7	-94.9	-12.8	91.9	3.13	4.64	10.60	1.70	54	3.2 ± 1.7	1.9 ± 0.2	-10.3	≤ 18	0.1 ± 0.1	NA	16.9
1σ error	± 1.5	± 0.1	$\pm 1\%$	$\pm 1\%$	$\pm 1\%$	$\pm 1\%$	$\pm 1.5\%$	± 3			± 0.4				$\pm 3\%$

mon excess air component found in groundwater (12, 13). Groundwater ages were determined from the ^{14}C activities of the total dissolved inorganic carbon. Conventional correction models (14) using chemical and isotopic balances were applied to convert activity values into ^{14}C ages. Conversion into calibrated years before present (B.P.) is based on (15).

Only the water from the recharge area (borehole 0) contains significant amounts of ^3H (half-life, 12.4 years) and ^{85}Kr (half-life, 10.8 years). The ^3H and ^{85}Kr values indicate a mean residence time of 15 years. Water from three boreholes (2, 4, and 6) turned out to be binary mixtures of an older and a younger component (Table 2). The proportion and residence time of the younger component were determined by measuring the concentrations of Cl^- and of the radioactive isotopes ^3H and ^{39}Ar (half-life, 269 years) (16). The presence of atmospheric ^{39}Ar and the absence of ^3H in the samples from boreholes 2, 4, and 6 (Table 1) imply that the younger component has a residence time of a few hundred years. The ^{14}C ages and NGTs

of the older component in these samples were calculated by correcting for the younger component. This correction is the cause of the large uncertainty in the ^{14}C ages at boreholes 2, 4, and 6. In the following, calibrated ^{14}C ages, NGTs, and $\delta^{18}\text{O}$ values refer only to the older component.

The NGTs vary significantly with time (Fig. 2). NGTs of groundwater samples younger than 7000 years (7 ky) agree with the recent mean annual air temperature of 8.3°C in the recharge area (17) and demonstrate the validity of the noble gas "thermometer" for modern climate. The intermediate NGTs at boreholes 2 and 4 are most likely the results of dispersive mixing within the aquifer under a climatic transition to present-day conditions. The lower NGTs of the samples with ^{14}C ages of 15 ky B.P. (borehole 3) and around 28 ky B.P. (boreholes 5 and 7) indicate a climate that was 5°C colder than it is now. During the last glacial maximum (around 18 ky B.P.) (18), the temperature drop may have been even greater than 5°C, but no samples with ages between 25 and 17 ky B.P. were found. An indication of a similar age gap has also been found in a study of a Triassic sandstone aquifer in England (19). In our study, it is unlikely that insufficient spatial resolution of the sampling boreholes is responsible for the observed age gap. Borehole 5 (27 ky B.P.) and borehole 3 (15 ky B.P.) are separated by less than 1 km along the direction of the flow. Adopting the mean observed flow velocity of 0.4 m year⁻¹ between boreholes 0 and 3, 1 km corresponds to an age increase of only 2.5 ky. The gap is therefore interpreted to be the result of an almost complete cessation of groundwater recharge between 25 and 17 ky B.P. The inference that groundwater formation was interrupted during the last glacial maximum is consistent with the glaciological and climatological history of the Glatt Valley and adjacent areas: The Glatt Valley was ice-free before 28 ky B.P. and after 14.5 ky B.P. (5). The climate was dry and cold between about 33.5 and 28.5 ky B.P. (5), during which time infiltration may have been reduced or even interrupted. However, enhanced biological activity around 28 ky B.P. (5), corresponding to the age of the samples from boreholes 5 through 7, indicates the occurrence of a brief

warm period during which infiltration was possible.

The curve in Fig. 2 is derived from a model based on the following assumptions: (i) the temperature evolution during the last 30 ky in central Europe is similar to that derived from $\delta^{18}\text{O}$ measurements in Greenland ice cores (20); (ii) the maximum $\delta^{18}\text{O}$ change corresponds to a temperature decrease of 8.6°C relative to present-day conditions (4, 21); (iii) the recharge rate is constant except between 25 and 17 ky B.P., when recharge is assumed to be zero; and (iv) the dispersivity of the water flow in the GVA is 100 m, which is representative of an aquifer of the size of the GVA (22). The model and noble gas data correspond well with ^{14}C ages up to 15 ky B.P., strengthening our confidence in the ^{14}C dating. However, for the older groundwaters around 28 ky B.P. the NGTs exceed the model predictions. Lithological profiles (5) and Greenland $\delta^{18}\text{O}$ ice records (20) consistently point to dramatic temperature fluctuations during the Denekamp Interstadial (18 to 33 ky B.P.). If groundwater recharge was interrupted during colder intervals, the NGTs would selectively reflect the signals of the warmer periods, which could explain the deviation from the model.

All $\delta^2\text{H}$ and $\delta^{18}\text{O}$ values (Tables 1 and 2) lie close to the global regression line of $\delta^2\text{H} = 8.2 \delta^{18}\text{O} + 10.8$ (23), which indicates that $\delta^{18}\text{O}$ was not modified significantly by isotope exchange within the aquifer. We corrected the $\delta^{18}\text{O}$ values for the variation in the isotopic composition of seawater due to increased ice volume (24). The calculated slope of the linear fit to the $\delta^{18}\text{O}$ and NGT data (25), which represents the long-term $\delta^{18}\text{O}$ -temperature relation in the recharge area, is 0.49 ± 0.17 per mil (‰) per °C (Fig. 3). This slope is in good agreement with both the present-day spatial (0.56 ‰ per °C) and seasonal (0.45 ‰ per °C) slopes for the Swiss Plateau (26). This finding should help in the interpretation of stable isotope data from other archives as temperature proxies.

References and Notes

1. J. Rudolph, H. K. Rath, C. Sonntag, in *Isotope Hydrology 1983* (International Atomic Energy Agency, Vienna, 1984), pp. 467-477; M. Stute, P. Schlosser, J. F. Clark, W. S. Broecker, *Science* **256**, 1000 (1992); J. N. Andrews et al., *Water Resour. Res.* **30**, 45 (1994).
2. M. Stute, J. F. Clark, P. Schlosser, W. S. Broecker, *Quat. Res.* **43**, 209 (1995).
3. M. Stute et al., *Science* **269**, 379 (1995).
4. M. Stute, C. Sonntag, J. Déak, P. Schlosser, *Geochim. Cosmochim. Acta* **56**, 2051 (1992).
5. C. Schlüchter et al., *Vierteljahresschr. Naturforsch. Ges. Zürich* **132**, 135 (1987).
6. G. S. Boulton, P. E. Caban, K. Van Gijssel, *Quat. Sci. Rev.* **14**, 545 (1995); J. A. Piotrowski, *Sediment. Geol.* **111**, 217 (1997).
7. K. O. Münnich and J. C. Vogel, *Geol. Rundsch.* **52**, 611 (1962); E. T. Degens, *ibid.*, p. 625.

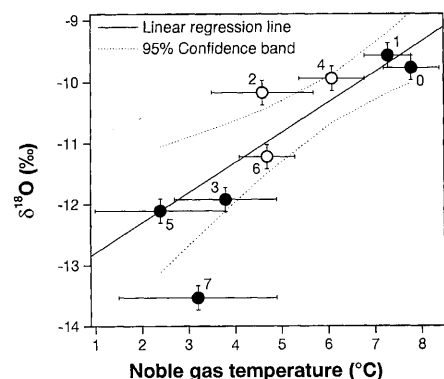


Fig. 3. Relation between $\delta^{18}\text{O}$ and NGT. Error bars correspond to 1σ . The sample numbers refer to the boreholes shown in Fig. 1. Solid circles indicate samples without mixture. For samples containing a mixture of an older and a younger component (open circles), the values shown refer to the older component only. The $\delta^{18}\text{O}$ shift in the ocean during the ice age (24) is taken into account. The slope of the $\delta^{18}\text{O}$ -NGT regression line inferred from the corrected $\delta^{18}\text{O}$ data is 0.49 ± 0.17 ‰ per °C (25), which agrees with the present-day $\delta^{18}\text{O}$ -temperature spatial and seasonal relations (26).

Table 2. Proportion of the younger component (16) and corrected data for the older component of mixed samples. Noble gas concentrations and stable isotope ratios for the older component were calculated by assuming that the younger component had the same composition as the sample from borehole 0.

Borehole	Proportion of the younger component (%)	Corrected data for the older component		
		$\delta^2\text{H}$ (‰)	$\delta^{18}\text{O}$ (‰)	NGT (°C)
2	35 ± 5	-71.9 ± 2.5	-10.1 ± 0.2	4.6 ± 1.1
4	50 ± 5	-72.4 ± 3.4	-9.8 ± 0.2	6.1 ± 0.7
6	8 ± 5	-74.8 ± 1.7	-10.6 ± 0.1	4.7 ± 0.6

8. E. Mazor, *Geochim. Cosmochim. Acta* **36**, 1321 (1972).

9. Stable isotope composition in groundwaters is controlled by the temperature and humidity prevailing during evaporation and during the condensation of precipitation, and by the large-scale atmospheric circulation patterns. It can later be altered by local evaporation, by mixing with melting ice or snow, and by water-rock interaction within the aquifer [M. Mazor, in *Chemical and Isotopic Groundwater Hydrology* (Dekker, New York, 1997), chap. 9].

10. M. Stute and P. Schlosser, in *Climate Change in Continental Isotopic Records*, P. K. Swart, K. C. Lohmann, J. McKenzie, S. Savin, Eds. (American Geophysical Union, Washington, DC, 1993), vol. 78, pp. 89–100.

11. L. Wyssling, *Hydrogeologische Erforschung des tief-liegenden Grundwasserstromes im oberen Glattal/ZH* (Report number 88.46, Office of Public Works (Baudirektion) of the Canton of Zürich, Department of Water Protection, Zürich, 1988).

12. J. N. Andrews, in *Isotopes of Noble Gases as Tracers in Environmental Studies* (International Atomic Energy Agency, Vienna, 1992), pp. 87–110; T. H. E. Heaton and J. C. Vogel, *J. Hydrol.* **50**, 201 (1981).

13. The processes responsible for this excess of atmospheric gases are not yet fully understood. Some experimental data indicate that the elemental ratios of the noble gas excesses correspond to the composition of unfractionated atmospheric air (2). A more sophisticated correction scheme, accounting for a fractionation of the excess air, has been proposed for cases when otherwise no consistent temperatures can be obtained from the different noble gases (3). In our study, the common correction with an excess of atmospheric composition yields coherent results, and no additional correction for fractionation is required.

14. E. Ingerson and F. J. Pearson, in *Recent Researches in the Fields of Atmosphere, Hydrosphere and Nuclear Geochemistry* (Nagoya University, Nagoya, Japan, 1964), pp. 263–283; J. C. Fontes and J. M. Garnier, *Water Resour. Res.* **15**, 399 (1979).

15. M. Stuiver and P. J. Reimer, *Radiocarbon* **35**, 215 (1993); E. Bard, B. Hamelin, R. G. Fairbanks, A. Zindler, *Nature* **345**, 405 (1990).

16. For each borehole j , the following three balance equations can be defined:

$$C_{k,s}^j = x^j \cdot C_{k,y}^j + (1 - x^j) \cdot C_{k,o}^j$$

where x^j is the mixing ratio of the younger component and C_k^j is the concentration or activity ($k = \text{Cl}^-$, ^{39}Ar , or ^{14}C) of the sample (s), of the younger component (y), and of the older component (o). To allow the calculation of x^j , it was assumed that (i) the ^{14}C activity of the younger component is similar to the calculated initial activity of the sample; (ii) the dissolved inorganic carbon concentrations in the two components are comparable; (iii) the subsurface background ^{39}Ar equilibrium activity is constant in the whole aquifer (an assumption supported by constant ^{222}Rn and ^{37}Ar activities) and given by the lowest measured values at boreholes 1, 3 and 7 [~10% modern (Table 1)]; (iv) the older component contains no atmospheric ^{39}Ar ; and (v) the ^{39}Ar activity and the Cl^- concentration of the younger component are the same in all samples.

17. M. Schüepf, in *Atlas der Schweiz*, E. Spiess, Ed. (Verlag der Eidgenössischen Landestopographie, Wabern-Bern, Switzerland, 1981), p. 11.

18. CLIMAP, *Science* **191**, 1131 (1976).

19. A. H. Bath, W. M. Edmunds, J. N. Andrews, in *Isotope Hydrology 1978* (International Atomic Energy Agency, Neuhberg, Vienna, 1979), vol. 2, pp. 545–568.

20. S. J. Johnsen, D. Dahl-Jensen, W. Dansgaard, N. Gundestrup, *Tellus* **47B**, 624 (1995).

21. B. Frenzel, in *Das Klima*, H. Oeschger, B. Messerli, M. Svilar, Eds. (Springer-Verlag, Berlin, 1980), pp. 45–63.

22. L. W. Gelhar, C. Welty, K. R. Rehfeldt, *Water Resour. Res.* **28**, 1955 (1992); A. Zuber, *J. Hydrol.* **86**, 45 (1986).

23. Y. Yurtsever and J. R. Gat, in *Stable Isotope Hydrology: Deuterium and Oxygen-18 in the Water Cycle*, J. R. Gat and R. Confiantini, Eds. (International Atomic Energy Agency, Vienna, 1981), pp. 103–142.

24. T. Sowers et al., *Paleoceanography* **8**, 737 (1993).

25. The data from borehole 7 have been disregarded

because the low $\delta^{18}\text{O}$ value and large excess air component of this sample (Table 1) may indicate that meltwater infiltrated during the short warmer climate period around 28 ky B.P. This might also account for the somewhat disturbed noble gas pattern, which results in a relatively large error in the calculated NGT at borehole 7.

26. U. Siegenthaler and H. Oeschger, *Nature* **285**, 314 (1980); M. Kullin and H. Schmassmann, in *Applied Isotope Hydrogeology, a Case Study in Northern Switzerland*, F. J. Pearson et al., Eds. (Elsevier, Amsterdam, 1991), pp. 65–89.

27. W. Aeschbach-Hertig, F. Peeters, U. Beyerle, R. Kipfer, *Water Resour. Res.*, in preparation; noble gas solubilities are from R. F. Weiss, *Deep-Sea Res.* **17**, 721 (1970); *J. Chem. Eng. Data* **16**, 235 (1971); H. L.

Clever, Ed., in *Krypton, Xenon and Radon—Gas Solubilities* (Pergamon, Oxford, 1979), pp. 1–226.

28. J. N. Andrews et al., in *Isotope Hydrology 1983* (International Atomic Energy Agency, Vienna, 1984), pp. 535–576; H. H. Loosli, B. E. Lehmann, G. Däppen, in *Applied Isotope Hydrogeology, a Case Study in Northern Switzerland*, F. J. Pearson et al., Eds. (Elsevier, Amsterdam, 1991), pp. 153–174.

29. This project was supported by the Swiss National Science Foundation (project no. 20-47060.96). We thank H. Baur, T. Graf, M. Möll, and S. Reese for assisting in the measurements; E. Hoehn for discussions; an anonymous reviewer for his or her comments; and D. Livingstone for linguistic improvements in the text.

3 June 1998; accepted 21 September 1998

Self-Organized Growth of Three-Dimensional Quantum-Dot Crystals with fcc-Like Stacking and a Tunable Lattice Constant

G. Springholz,* V. Holy, M. Pinczolits, G. Bauer

The self-organization of pyramidal PbSe islands that spontaneously form during strained-layer epitaxial growth of PbSe/Pb_{1-x}Eu_xTe ($x = 0.05$ to 0.1) superlattices results in the formation of three-dimensional quantum-dot crystals. In these crystals, the dots are arranged in a trigonal lattice with a face-centered cubic (fcc)-like A-B-C-A-B-C vertical stacking sequence. The lattice constant of the dot crystal can be tuned continuously by changing the superlattice period. As shown by theoretical calculations, the elastic anisotropy in these artificial dot crystals acts in a manner similar to that of the directed chemical bonds of crystalline solids. The narrow size distribution and excellent control of the dot arrangement may be advantageous for optoelectronic device applications.

Semiconductor nanostructures have attracted tremendous interest in the past few years because of their special physical properties and their potential for applications in micro- and optoelectronic devices (1). In such nanostructures, the free carriers are confined to a small region of space by potential barriers, and if the size of this region is less than the electron wavelength, the electronic states become quantized at discrete energy levels. The ultimate limit of low dimensional structures is the quantum dot, in which the carriers are confined in all three directions. Therefore, a quantum dot can be thought of as an artificial atom. The fabrication of quantum dots presents a formidable challenge because the small dimensions required for quantum dots are at the limit of lithographic and semiconductor processing techniques and also because the dot interfaces must be kept defect-free in order to obtain the

high-quality electronic properties that are required for device applications. As a consequence, many efforts have been made to develop alternative routes for the fabrication of quantum dots that are based on the principle of self-organization (1–4).

The spontaneous formation of three-dimensional (3D) islands in strained-layer heteroepitaxy has recently emerged as a new technique for the synthesis of self-assembled quantum dots (3–6). This technique is based on the fundamental morphological instability of strained surfaces, which is driven by the elastic relaxation of strain energy in the freestanding islands that spontaneously nucleate on the surface of a growing epitaxial layer after the completion of the wetting layer (7). In the early stage of growth, these islands are defect-free and fully coherent to the substrate (8). Therefore, quantum dots are obtained in situ without the interface problems that are associated with ex situ processing techniques. However, although single quantum dots exhibit extremely sharp, atomic-like luminescence properties (5, 9), the considerable inhomogeneous line broadening in larger dot ensembles due to nonuniformities in the dot sizes has posed considerable limitations for device applications (6, 10).

G. Springholz, M. Pinczolits, G. Bauer, Institut für Halbleiterphysik, Johannes Kepler Universität Linz, 4040 Linz, Austria. V. Holy, Laboratory of Thin Films and Nanostructures, Faculty of Science, Masaryk University, Kotlarska 2, 611 37 Brno, Czech Republic.

*To whom correspondence should be addressed. E-mail: g.springholz@hphys.uni-linz.ac.at